The EMBO Journal Vol. 21 No. 22 pp. 6146–6153, 2002

From chloroplasts to photosystems: *in situ* scanning force microscopy on intact thylakoid membranes

David Kaftan[1,2], Vlad Brumfeld[1], Reinat Nevo[3], Avigdor Scherz[1] and Ziv Reich[3,4]

[1]Department of Plant Sciences and [3]Department of Biological Chemistry, Weizmann Institute of Science, Rehovot 76100, Israel and [2]Centre for Photosynthesis, Laboratory of Applied Photobiology and Bio-Imaging, Institute of Landscape Ecology, Zámek 136, 37333 Nové Hrady, Czech Republic

[4]Corresponding author
e-mail: ziv.reich@weizmann.ac.il

Envelope-free chloroplasts were imaged *in situ* by contact and tapping mode scanning force microscopy at a lateral resolution of 3–5 nm and vertical resolution of ~0.3 nm. The images of the intact thylakoids revealed detailed structural features of their surface, including individual protein complexes over stroma, grana margin and grana-end membrane domains. Structural and immunogold-assisted assignment of two of these complexes, photosystem I (PS I) and ATP synthase, allowed direct determination of their surface density, which, for both, was found to be highest in grana margins. Surface rearrangements and pigment–protein complex redistribution associated with salt-induced membrane unstacking were followed on native, hydrated specimens. Unstacking was accompanied by a substantial increase in grana diameter and, eventually, led to their merging with the stroma lamellae. Concomitantly, PS IIα effective antenna size decreased by 21% and the mean size of membrane particles increased substantially, consistent with attachment of mobile light-harvesting complex II to PS I. The ability to image intact photosynthetic membranes at molecular resolution, as demonstrated here, opens up new vistas to investigate thylakoid structure and function.

Keywords: membrane stacking/photosystems/scanning force microscopy/state transitions/thylakoid structure

Introduction

Photosynthesis in green plants takes place in chloroplasts, semi-autonomous organelles found predominantly in leaf cells. The key structural component of the chloroplast is a membranous continuum of flattened vesicles called thylakoids, which host all functional protein and pigment–protein complexes necessary for the light-driven reactions of photosynthesis. In most vascular plants and some green algae, the thylakoids are differentiated into two distinct membrane domains, cylindrical stacked structures, known as grana, and interconnecting single membrane regions, called stroma lamellae. The stroma lamellae and the end and side membranes of the grana face an aqueous matrix termed the stroma, which is located between the chloroplast inner envelope membrane and the thylakoids (Staehelin and van der Staay, 1996).

Our understanding of the structure of isolated photosystems and light-harvesting complexes (LHCs) from oxygen-evolving organisms has increased tremendously over the past few years (Kuhlbrandt *et al*., 1994; Kitmitto *et al*., 1998; Jordan *et al*., 2001; Zhouni *et al*., 2001). This information can now be incorporated into low-resolution models of thylakoid structure available from serial thin section reconstructions (Mustardy and Brangeon, 1978), freeze etching of tag-free (Staehelin, 1976) and immunogold-labelled specimens (Olive and Vallon, 1991), and from spectroscopic analyses of whole and fragmented thylakoid preparations (Albertsson and Yu, 1988).

The two photosystems are spatially segregated in the thylakoids (reviewed in Albertsson, 2001). Photosystem I (PS I) and the light-harvesting chlorophyll *a/b* pigment–protein I (LHC I) localize to stroma lamellar domains, grana-end membranes and grana margins. Photosystem II (PS II) and its associated LHC (LHC II), on the other hand, concentrate almost exclusively in the stacked regions of the grana interior. Each of the photosystems also gives rise to two subpopulations (referred to as α and β) with distinct localization, LHC content and, probably, functionality. The cytochrome b_6/f complex and the CF_0F_1 ATP synthase are also distributed non-homogeneously over the membranes, with the former preferentially populating grana-appressed regions and grana margins, and the latter regions enriched in PS I.

The multipartite organization of the photosynthetic apparatus is probably important for its steady-state function and is essential for its ability to adapt to changes in light quality and intensity on distinctively diverse time scales (Trissl and Wilhelm, 1993). However, many details concerning the spatial distribution and stoichiometry of the various protein complexes within the intact thylakoid membranes remain unknown. How these properties change during the various adaptive processes is also unclear. Electron microscopy (EM), which has proved invaluable to the field, is not compatible with high-resolution studies of whole mounts under native conditions. On the other hand, fluorescence-based techniques, while capable of providing information regarding the microconnectivity between the different particle species, lack the ability to localize them accurately within the membrane.

In this work, we used scanning force microscopy (SFM; Binnig *et al*., 1986) to image the surface of intact, chemically fixed and native hydrated thylakoid membranes within de-enveloped chloroplasts. Optimizing imaging parameters, we could acquire images on fixed samples at 3–5 nm lateral resolution and ~0.3 nm vertical resolution. This high resolution enabled us to resolve

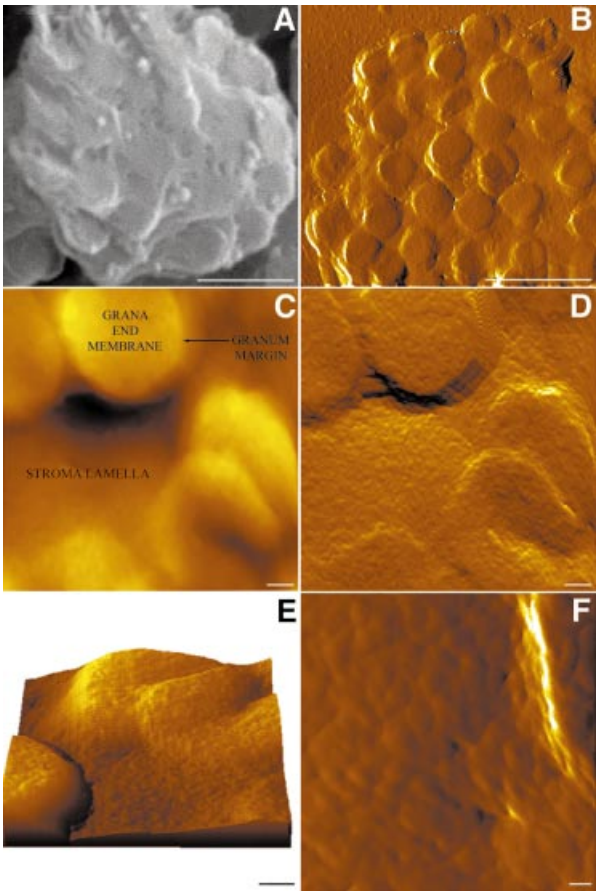

Fig. 1. Chemically fixed intact thylakoids imaged by SEM (**A**) and SFM (**B**–**F**). (B), (D) and (F) are error images; (C) is a height image; (E) is a three-dimensional rendering of the surface. Grana-end membranes are visible as circular protrusions of the undulating stroma regions; connectivity between the stroma lamellae and grana surfaces is apparent at both the grana top and bottom. The individual particles shown in (F) are mostly PS I complexes. The ridge observed on the right side of the image represents a granum margin. Scale bars are 1 μm in (A) and (B), 100 nm in (C–E) and 25 nm in (F); the full intensity range in (C) is 450 nm.

individual protein complexes over both stroma and grana-end membranes. Two of these complexes, ATP synthase and PS I, have also been immunogold labelled, and their surface distribution was determined over different thylakoid domains. Untreated, photosynthetically active preparations were used to follow surface rearrangements associated with membrane unstacking induced by divalent cation depletion. Changes in surface topography were accompanied by a significant drop in PS II antenna size and by an increase in the size of protein complexes located in the stromal domains. These findings are consistent with the translocation of grana-localized LHC II molecules into the stroma lamellae and their attachment to PS I (Allen and Forsberg, 2001).

Results

We set out to image intact thylakoid membranes under conditions as close as possible to *in vivo*. As imaging by the SFM requires contact between the SFM probe (tip) and the surface of the sample, we used de-enveloped (class II) chloroplasts which have lost their two enveloping membranes, but preserve their internal organization and photochemical activity (Avron, 1960). We assessed the latter from the maximum photochemical yield of PS II, Φ_p^{max}, derived from measurements of chlorophyll fluorescence (Genty *et al*., 1989). In suspension, freshly isolated class II chloroplasts had a mean Φ_p^{max} of 0.64 ± 0.02. Adsorption of the membranes over a glass substrate, to mimic conditions used for the SFM analyses, slightly decreased Φ_p^{max} to 0.55 ± 0.08.

Scanning EM of de-enveloped chloroplasts

Scanning electron micrographs of envelope-free chloroplasts show a clear, intact thylakoid morphology with distinct stromal and granal (flattened disks with a diameter of 500 ± 28 nm) regions; the former appear as thin strips interconnecting neighbouring grana (Figure 1A). The shape and dimensions of the thylakoids, as well as of the constituent domains, agree well with previously published electron (Staehelin and van der Staay, 1996) and confocal (Mehta *et al*., 1999) microscopy data. With the resolution attained (pixel size corresponds to ~10 nm), individual protein complexes cannot be resolved over the membrane surfaces, which appear relatively smooth.

Contact mode scanning force microscopy of fixed thylakoids

Dark-adapted, chemically fixed (de-enveloped) chloroplasts were imaged using contact mode SFM. A low-magnification image of such a chloroplast is shown in Figure 1B. It appears as an ellipsoidal-shaped structure, 3.5 μm in length and 3 μm in width, similar to the appearance of natively isolated chloroplasts under the light microscope (data not shown). Its height, however, is significantly reduced compared with that of an enveloped chloroplast (0.45 versus 1 μm) due to the loss of the large aqueous space of the stromal compartment. The measured grana dimensions (450 ± 30 nm) are consistent with the EM data reported here and by others (Staehelin and van der Staay, 1996).

At higher magnification, additional features of the surface become apparent. Figure 1C presents a high-magnification topograph, showing the surface of individual grana as well as of the interconnecting stroma lamellae. Surface features are discerned even better in the error image shown in Figure 1D. The stroma lamellae become more visible and, with that, the stroma–grana boundaries. A three-dimensional rendering of the surface shown in Figure 1C is depicted in Figure 1E. The image reveals that, while some stromal lamellae are connected to the grana at their top, others adjoin the grana at their bottom, ~100 nm below the surface. Such a mode of connectivity is consistent with a continuous helical model of the thylakoid, as proposed by Mustardy, 1996.

Particle distribution over the thylakoid membranes

In addition to detailing the overall thylakoid fold, the SFM images also reveal elliptically shaped particles over both grana and stromal lamellae regions (Figure 1C–F). The results obtained by deconvoluting the particle size versus height histograms into individual particle classes are shown in Figure 2. The shape, size and height of the particles, combined with the fact that we can only visualize grana-end membranes and stroma lamellae

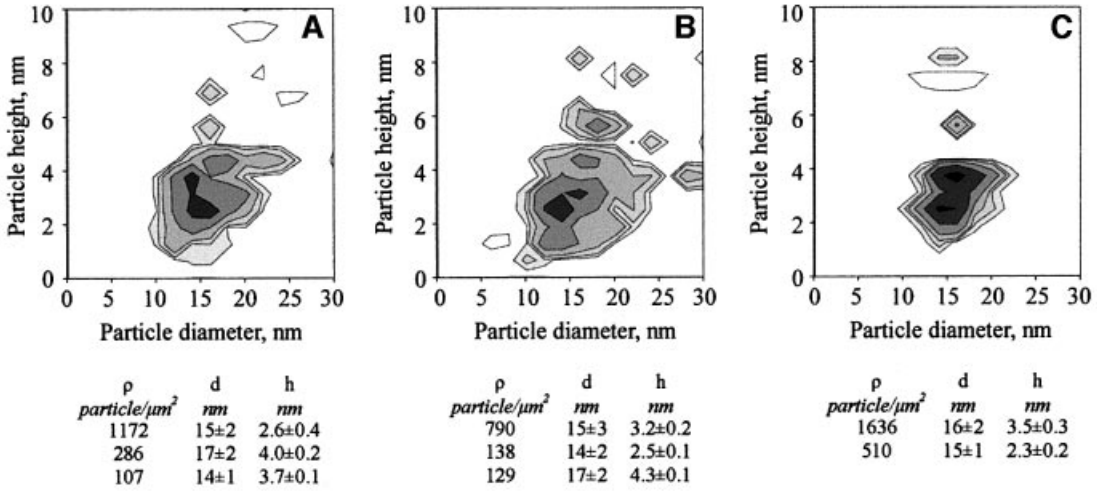

ρ particle/μm²	d nm	h nm
1172	15±2	2.6±0.4
286	17±2	4.0±0.2
107	14±1	3.7±0.1

ρ particle/μm²	d nm	h nm
790	15±3	3.2±0.2
138	14±2	2.5±0.1
129	17±2	4.3±0.1

ρ particle/μm²	d nm	h nm
1636	16±2	3.5±0.3
510	15±1	2.3±0.2

Fig. 2. Distribution of surface particles over different thylakoid domains presented as contour plots of particle size versus height histograms. (**A**) Stroma lamellae. (**B**) Grana-end membranes. (**C**) Grana margins. The contour step is 20 particles/μm^2. Histograms were fitted with a sum of Gaussian peaks by least square numerical fitting. Classes of particles assigned as PS I are listed below the frames.

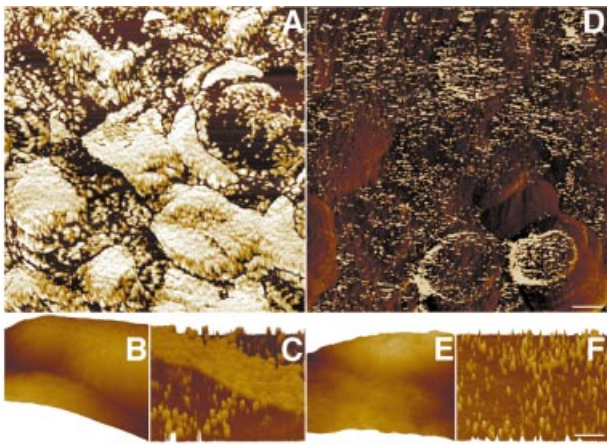

Fig. 3. Surface distribution of immunogold-labelled PS I (**A**–**C**) and ATP synthase (**D**–**F**) complexes. (A and D) Phase images. (B and E) Three-dimensional renderings. (C and F) Phase images of the areas shown in (B) and (E). Note that the *z*-axis in the phase images corresponds to a phase shift between the cantilever response and the driving signal, and does not represent the height of the surface. Scale bars: 200 nm in (A) and (D); 100 nm in (B), (C), (E) and (F).

regions where PS I is abundant, strongly suggest that most of them are PS I complexes. A notable feature of the histograms is that the number of particles with characteristics expected for the CF_0F_1 ATP synthase is exceedingly small. The latter should occupy a unique position in the two-dimensional maps since it should protrude well above the plane of the membranes, even if a substantial decrease in height is expected due to dehydration and the consequent collapse of the stromal exposed catalytic unit. The reason for this absence of ATP synthase from the images acquired in the contact mode is discussed later.

We next classified the prominent particle species we assigned as PS I complexes according to their height. Unlike lateral dimensions, which can be overestimated because of tip convolution, the height of objects determined by SFM is not affected by this effect. As indicated (Figure 2), in each topological domain, two classes dominate the surface. The first exhibits height values expected for intact PS I, i.e. between 3.2 and 4.0 nm. Particles belonging to this class have a surface density of ~400, 800 and 1600 particles/μm^2, over stroma lamellae, grana end-membranes and grana margins, respectively. Particles of the second class have essentially identical lateral dimensions and shape to those belonging to the first group, but exhibit a significantly reduced height (2.3–2.6 nm). Interestingly, these latter particles, which we interpret as PS I molecules lacking one or more extrinsic subunits (i.e. PsaC, D or E), are particularly prevalent over the stroma lamellae where they actually dominate the surface. The surface density of these particles is ~1200 (stroma lamellae), 150 (grana-end membranes) and 500 (grana margins) particles/μm^2. Both particle classes exhibit variations in the lateral dimension of their constituents, ranging from 14 to 17 nm.

Tapping mode SFM of immunolabelled thylakoids

In contact mode SFM, the cantilevered probe (tip) is translated over the sample so it is continuously touching the surface. Consequently, this mode is associated with substantial shear forces, which can damage the sample, in particular if it is relatively soft or fragile. This problem can be overcome effectively by using dynamic (A/C) imaging modes, called tapping or intermittent-contact modes. These modes, which use near-resonance, vertical oscillation of the SFM cantilever, virtually eliminate shear forces during scanning. In addition, these modes are highly sensitive to the local mechanical properties of the surface, allowing for easy discrimination between low- and high-modulus materials. We utilized this latter fact selectively to visualize PS I and ATP synthase complexes labelled with gold-conjugated secondary antibodies. Primary antibodies were against the stromal-exposed PsaD subunit of PS I and the β subunit of the CF_1 complex of the ATP synthase. A map of gold-labelled PS I is shown in Figure 3A. Clearly, the distribution of this complex is non-homogeneous, ranging from >1500 particles/μm^2 over

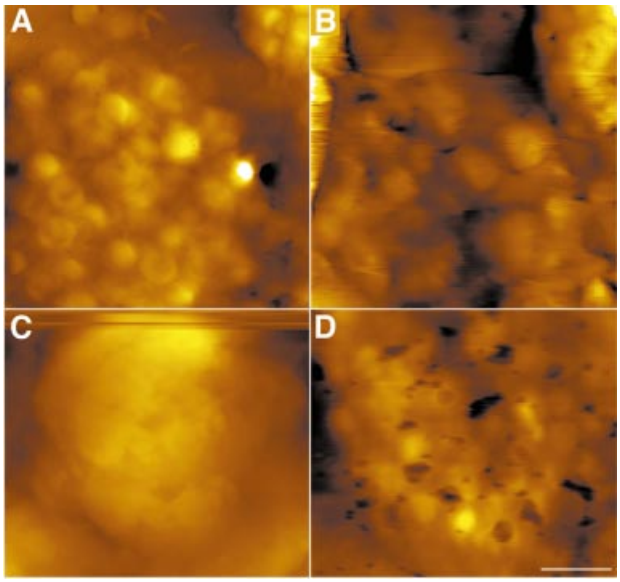

Fig. 4. Grana unstacking imaged on native, hydrated thylakoids. An increase in grana size is observed. Native thylakoid membranes (**A**) were subjected to 50 (**B**) or 100 (**C**) mM EDTA. For re-stacking, samples treated with 100 mM EDTA were incubated in a medium containing 5 mM Mg^{2+} (**D**). Evidently, the original membrane organization has been restored. Because repetitive scans over long periods damaged the thylakoids, images were obtained from different samples. The scale bar is 1 μm.

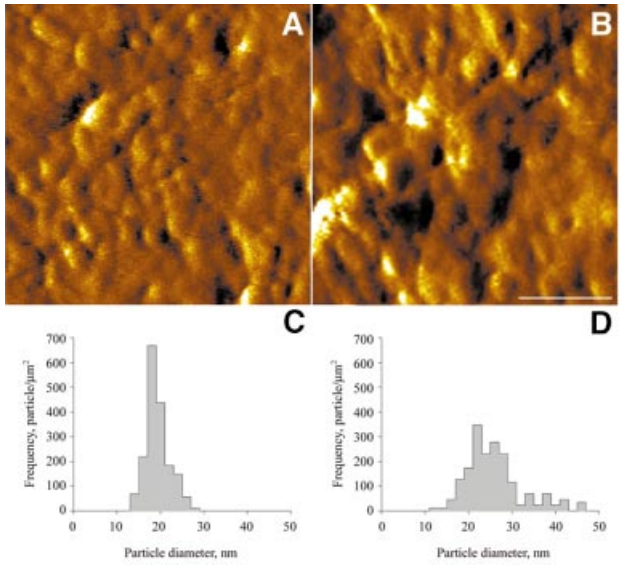

Fig. 5. High-resolution images of native thylakoids in the absence (**A**) and presence (**B**) of 100 mM EDTA. Going from the control (**C**) to the EDTA-treated sample (**D**), a substantial increase in particle size is apparent. The scale bar is 100 nm.

grana margins, through ~700 particles/μm^2 over grana-end membranes, to ~400 particles/μm^2 over the stroma lamellae. These differences in surface density are also illustrated in Figure 3C, which presents a high-magnification three-dimensional rendering of a grana margin–stroma lamella boundary. While the stroma lamella (lower part) is only moderately labelled, the adjacent grana margin, corresponding to the central transverse part of the map, is labelled heavily. Notably, the above values of PS I density are in excellent agreement with those derived structurally for particles exhibiting intact PS I morphology (Figure 2).

The differences in surface distribution of gold-labelled ATP synthase are somewhat less pronounced. This complex also appears less abundant than PS I over most membrane domains. As shown (Figure 3D–F), individual, almost evenly distributed, CF_1 complexes are labelled over the stroma lamellae and grana-end membranes. Over these regions, the synthase exhibits similar density of ~400 particles/μm^2. Like PS I, it is also concentrated mostly in the grana margins, where it reaches a density of ~600 particles/μm^2.

In situ unstacking of unfixed thylakoid membranes

A representative low-magnification image of unfixed thylakoids in Mg^{2+}-containing buffer is shown in Figure 4A. Compared with their morphology in the fixed preparations, the native grana appear more circular, with an average diameter of 361 ± 63 nm. The apparent chloroplast height is 400 nm, similar to that measured under fixation conditions. The effect produced by treating the samples with 50 mM EDTA is illustrated in Figure 4B. Consequent to such a treatment, the lateral dimensions of the grana increased substantially, averaging now 720 ± 48 nm, about twice the size measured in the absence of EDTA. The shape of the grana changed too, becoming more ellipsoidal and losing structural regularity. The protrusion height of the grana (i.e. the distance between the granum top and the nearest stroma lamella surface), however, did not change above the experimental errors, remaining at 48 ± 10 nm. When the EDTA concentration was raised further, to 100 mM, a complete unstacking of the membranes occurred (Figure 4C), with structures similar to grana no longer distinguishable from the stromal lamellae domains. Incubation of the 100 mM EDTA-treated samples in a buffer containing 5 mM $MgCl_2$ restored the native membrane organization (Figure 4D); the average grana diameter now standing at 405 ± 40 nm.

The aforementioned structural alterations were correlated to the photochemical parameters of the samples using two related functional measures, Φ_p^{max} and σ_{PSII}, the functional cross-section of PS II. The latter parameter was derived from analysis of chlorophyll fluorescence induction in the presence of 3-(3,4-dichlorophenyl)-1,1-dimethylurea (DCMU) (Melis and Homan, 1976). Treatment of the samples with 100 mM EDTA led to a 21 and 22% decrease in $\sigma_{PSII}\alpha$ and $\sigma_{PSII}\beta$, respectively. The relative abundance of grana-associated PS IIα dropped by 50%, concomitant with a corresponding increase in the PS IIβ population. Restacking the samples in a medium containing Mg^{2+} restored σ_{PSII} to 90% of its original value. Similarly, untreated specimens exhibited a mean Φ_p^{max} value of 0.55 ± 0.1, which decreased to 0.35 ± 0.1 upon the addition of 100 mM EDTA, marking a substantial loss of PS II activity. Incubation of the EDTA-treated samples in a 5 mM $MgCl_2$ solution yielded a $\Phi_{p\ PSII}$ of 0.47 ± 0.07.

Membrane unstacking was also associated with a significant change in the size of the particles over the membranes. Figure 5A and B shows the surfaces of grana-end membranes from untreated and EDTA-treated

samples acquired in the error mode. This (contact) mode was used since the images recorded on the native specimens in the height mode were of a relatively low quality, which did not allow for detailed analysis. An advantage of the error mode is that it is highly sensitive to subtle changes in surface relief and can often discern features not detected in the height mode. A drawback of this mode is that it cannot provide quantifiable height information. Analysis of the particles over the native membranes was therefore limited to lateral dimensions. As indicated in Figure 5C, the size distribution of membrane particles in the untreated sample is relatively narrow, with a peak centred at 18 nm. In contrast, the distribution of particles in the EDTA-treated samples is both broad and bi-modal, with the two maxima shifted to larger values of 21 and 27 nm (Figure 5D). A number of satellite peaks is also apparent, reaching values >40 nm.

Discussion

The structure of many isolated photosynthetic pigment–protein complexes has now been determined. However, a full understanding of the photosynthetic apparatus requires that the spatial localization, supramolecular organization and dynamics of the individual components within the thylakoid membranes also be known. With its ability to operate in liquids and exceptionally high S/N ratio, the SFM provides an ideal tool to address these issues. Obtaining high-resolution images of membrane structures and proteins by SFM, however, is challenging. To date, visualization of membrane proteins at subnanometre lateral resolution has been achieved only for molecules packed in two-dimensional crystalline arrays. In most other cases, resolution drops to a few nanometres for supported lipid bilayers, and to a few tens of nanometres for organelles and cells (Reich *et al*., 2001).

Here we were able to image the surface of intact thylakoids at lateral resolution of 3–5 nm and vertical resolution of ~0.3 nm which, following image analysis, might be sufficient to explore even substructural features of individual protein complexes. To enable access to the SFM tip, we used class II chloroplasts in which the external envelope membranes have been removed. These chloroplasts retained their native organization and photochemical activity, as shown by scanning EM and quantum yield of PS II electron transfer, respectively.

Low-magnification SFM images of envelope-free chloroplasts fully exposed the surface organization of the thylakoid membranes. Our data generally agree with previous descriptions of higher plant thylakoids by EM, but provide additional information regarding their surface topology and three-dimensional rendering. The latter allowed the coupling between the stromal and granal domains to be clearly defined. In particular, it shows that the two domains connect in a manner consistent with a continuous helical organization where the stroma lamellae exist in a spiral arrangement around the grana (Mustardy, 1996).

High-resolution topographs of the thylakoids allowed for the detection of individual protein complexes over the membranes. We assign most of these complexes as PS I. Early freeze-fracture studies of higher plant PS I indicated a diameter of 10–13 nm (Dunahay and Staehelin, 1985; Staehelin, 1986). In contrast, digital image analysis of negatively stained two-dimensional PS I crystals formed within spinach thylakoid grana margins yielded a value of 16 × 11 nm (Kitmitto *et al*., 1997). Measurements of detergent-solubilized spinach PS I set even larger dimensions (20 × 16 nm), but these were not corrected for attached detergent molecules (Boekema *et al*., 2001). The values presented in this work for the fixed preparations (Figure 2) are mostly in the middle of this range, with most of the particles having a diameter of ~15–16 nm. These values, however, correspond mostly to the PS I core, which protrudes well above the plane of the membranes. This part of the PS I–LHC I complex is therefore expected to dominate the images, with the less protruding LHC I molecules probably contributing little to the contour. It was proposed recently that green plant PS I is surrounded by four LHC I dimers, which are asymmetrically attached to the complex on one side (Boekema *et al*., 2001; Scheller *et al*., 2001). Integrating our data for PS I core into this model and using dimensions reported for LHC II (Kuhlbrandt *et al*., 1994) in place of LHC I, we come up with a value of 18/19 × 21/22 nm for such a PS I–4 (LHC I_2) supercomplex. This value is in excellent agreement with the 18 × 22 nm predicted for the structure. Compared with the fixed specimens, the average particle size measured over the native samples was consistently larger. This is expected since the latter were fully hydrated and thus retained a native, lower modulus, which decreases resolution and is often associated with a broadening effect.

About two-thirds of the particles we assigned as PS I molecules had an average height of 3.5 nm. This value is in excellent agreement with X-ray crystallography (Jordan *et al*., 2001) and SFM (Fotiadis *et al*., 1998) data showing a 3.5 nm ridge, containing the extrinsic PsaC, PsaD and PsaE subunits, over the stromal face of cyanobacterial PS I. However, a significant number of particles exhibited a much reduced height, in the range of 2.3–2.6 nm. This type of particle was particularly abundant over the stroma lamellae, where they actually dominated the surface. Such species, which we interpret as PS I complexes lacking one or more extrinsic subunits, might have been generated during scanning by the SFM tip. Similar observations were reported previously for cyanobacterial PS I packed in two-dimensional crystalline arrays (Fotiadis *et al*., 1998). The removal of peripheral components by the SFM stylus is probably also responsible for the failure to detect particles corresponding to the ATP synthase by contact mode SFM. The pronounced prevalence of particles with reduced height over the stroma lamellae suggests, however, that these regions may serve as repair sites for impaired PS I molecules.

The asymmetric distribution of photosynthetic complexes in the thylakoid membranes of higher plants is essential for the dynamic responsiveness of the photosynthetic apparatus to alternating environmental parameters such as varying light conditions (Anderson, 1999; Albertsson, 2001). An accurate determination of the distribution of these complexes over the thylakoid surface is therefore of major importance. Here, we provide the first quantitative determination of the surface distribution of PS I and ATP synthase over intact thylakoids. Based on structural assignment, the surface density of intact PS I

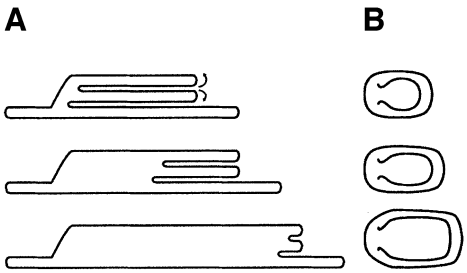

Fig. 6. A model of membrane unstacking. (**A**) Cross-section of the thylakoid stacks. (**B**) Top view. Unstacking begins by evagination of the membranes located at the stromal-exposed edges of the appressed grana domains (top). As unfolding proceeds, membranes are pulled from the stack's interior towards the edges, allowing for an increase in lateral dimensions with no change in height (middle and bottom). Eventually, the stacks merge completely with the neighbouring stroma lamellae, and grana topology is lost (Figure 4C).

molecules was found to be ~400, 800 and 1600 particles/μm^2 over the stroma lamellae, grana-end membranes and grana margins, respectively. These numbers closely match the values obtained from the immunogold maps, which indicate corresponding values of 400, 700 and 1500 particles/μm^2. Including species lacking one or more external subunits, the densities obtained are higher, i.e. 1600 (stroma lamellae), 900 (grana end-membranes) and 2100 (grana margins) particles/μm^2. These latter values are ~2-fold higher than those estimated for PS I molecules in spinach thylakoids (Albertsson, 2001).

Unlike the analysis made for PS I, our estimates of ATP synthase densities over the membranes rely solely on the results obtained from the immunogold maps and are thus likely to be underestimated. This limitation withstanding, the surface densities determined for this complex are ~400 particles/μm^2 over the stroma lamellae and grana end-membranes, and 600 particles/μm^2 over the grana margins. Thus, similarly to PS I, the ATP synthase appears to be most concentrated in the grana margins, implicating the latter as distinct structural and functional domains, as proposed (Albertsson, 2001).

Untreated, photochemically active thylakoids were used to follow surface rearrangements associated with the unstacking of the membranes by divalent cation depletion. This process has been studied intensively in connection with thylakoid organization and dynamics, and may have mechanics similar to those of light-induced unstacking generated during state I→state II transitions (Stys, 1995; Chow, 1999). The images provide the first visualization of this process on native thylakoid membranes. Application of increasing concentrations of EDTA was associated with marked increases in grana lateral dimensions leading, at a concentration of 50 mM, to a 2-fold increase in their size. The structural changes were paralleled by a decrease of the photosynthetic activity. Further depletion of the cations resulted in a complete loss of stacking, as judged by the disappearance of the appressed (granal) morphologies from the surface. The structural rearrangements induced by unstacking could be reversed upon the addition of Mg^{2+} ions to the samples, as indicated by the restoration of the stacked membrane morphology and Φ_p^{max}.

The direct observations we made on grana unstacking allowed us to draw a simple topological model for this process (Figure 6). As indicated, unstacking begins at the stromal-exposed edges of the appressed grana domains. This is followed by a gradual evagination of the membranes, leading to an increase in grana size, but leaving the height relatively constant (as observed). Evagination continues at similar rates in all of the stacks, such that the newly formed edges remain blunt like their appearance in the stacked state. Upon further destabilization of the membrane connections, evagination proceeds to completion, resulting in the merging of the unstacked regions with the membranes. This model is therefore different from previous models of grana unstacking, which invoke either a concomitant decrease in apparent grana size (Arvidsson and Sundby, 1999) or an increase in grana height due to electrostatic repulsion between poorly screened, negatively charged surfaces (Barber, 1980).

A prominent consequence of salt-induced grana unstacking is the randomization of PS I, PS II and LHC II within the membranes (Barber, 1980). In particular, the detachment of peripheral LHC II from PS II and their subsequent migration and association with PS I–LHC I has been implicated in the redistribution of excitation energy that follows the process (Allen and Forsberg, 2001). Our observation that the size of surface particles, assigned as PS I, increased upon unstacking is in accordance with such a transition. This is also consistent with data obtained from fluorescence induction experiments, which showed a significant decrease (~20%) in PS II functional cross-sections upon cation depletion (Boichenko, 1998). A similar change (~26%) in σ_{PSII} was observed in Mg^{2+}-depleted spinach thylakoids (Samson and Bruce, 1995). More recently, it was reported that unstacking of pea thylakoids by Mg^{2+} depletion increased PS I antenna size from ~200 to 370 chlorophyll molecules, consistent with the attachment of four LHC II trimers per PS I–LHC I complex (Boichenko, 1998). We thus tend to interpret the observed increase in particle size upon unstacking to result from the binding of mobile LHC II to PS I. However, the broad distribution of particle size in the unstacked samples precludes determination of the number of LHC II molecules that are bound. It also suggests that this number may not be fixed and that assemblies with different stoichiometries and/or composition are formed during the process.

Rearrangement of PS II and PS I units has been implicated in state I→state II transitions, which modulate the light energy distribution between the two photosystems (Drepper *et al*., 1993; Mullineaux *et al*., 1997). This mechanism is believed to operate via the reversible displacement of phosphorylated LHC II complexes from appressed granal partitions to stromal-exposed grana margins and stromal lamellar domains (Allen, 1992), where they are assumed to associate with PS I. Direct evidence for such an association, however, is missing. Moreover, recent observations showed that phosphorylation of thylakoid membranes, while decreasing the amount of O_2-evolving PS II units, did not lead to significant changes in their effective antenna size (Boichenko *et al*., 1997). We propose that the experimental strategy described in this work could be utilized to address these issues. More generally, this approach should

be useful to follow dynamic processes over native, intact photosynthetic membranes.

Materials and methods

Preparation of de-enveloped chloroplasts

Envelope-free chloroplasts were prepared according to Avron (1960), with a few modifications. Fresh lettuce leaves were blended in 0.2 M sucrose, 0.1 M NaCl, 50 mM Tricine–NaOH pH 8.0, 0.1 mM phenylmethylsulfonyl fluoride (PMSF), 1 mM ATP and 20 mM Na ascorbate (40 ml of grinding medium per 10 g of leaves) for 25 s. The slurry was filtered through four layers of miracloth and centrifuged for 90 s at 1000 *g*. The supernatant was then collected and centrifuged further for 10 min at 2000 *g*. Pellets were homogenized gently with a brush, and brought up to the original volume with a solution containing 0.2 M sucrose, 0.1 M NaCl, 1 mM ATP and 50 mM Tricine–NaOH pH 8.0. Following another centrifugation–resuspension cycle, supernatants were centrifuged for 10 min at 3000 *g*, and pellets were resuspended to a final concentration of 1 mg chlorophyll per ml in 0.3 M sucrose, 50 mM KCl, 5 mM $MgCl_2$, 1 mM ATP and 50 mM Tricine–NaOH pH 8.0. Chloroplasts were kept in the dark, on ice, and were used for experiments within 2 h of isolation. Chemicals were analytical grade and water was 18 MΩ/cm.

SFM

Samples were adsorbed onto glass coverslips cleaned by sonication in 50% acetone and washed thoroughly with water. Dried coverslips were incubated overnight (4°C) with 160 μM polylysine and washed with water. A 20 μl aliquot of isolated chloroplasts was spread homogeneously over the polylysine-coated coverslips and, following 15 min incubation, excess liquid was removed. Samples were rinsed three times with wash solution containing 50 mM KCl, 5 mM $MgCl_2$ and 50 mM Tricine–NaOH pH 8.0, and ice dried in the dark. Samples prepared for chemical fixation were exposed to 100 μl of a solution containing 2% glutaraldehyde, 50 mM KCl, 5 mM $MgCl_2$ and 50 mM Tricine–NaOH pH 8.0, for 15 min. This was followed by three successive incubations in 100 μl of the wash solution. For experiments involving membrane unstacking, Mg^{2+}-free solutions were used. Unstacking was induced by the application of 100 μl of Mg^{2+}-free wash solutions containing 50 or 100 mM EDTA, for 15 min. Subsequently, samples were washed three times with Mg^{2+}-free/EDTA-free solution. In the restacking experiments, the EDTA treatment was followed by a 15 min incubation with 100 μl of a wash solution containing 5 mM $MgCl_2$. For the immunogold labelling, specimens were immobilized on a glass and were fixed with 100 μl of a solution containing 0.5% glutaraldehyde, 4% paraformaldehyde, 300 mM sucrose, 50 mM KCl, 5 mM $MgCl_2$ and 50 mM Tricine–NaOH pH 8.0, for 30 min. Followed blocking (1 h) with 4% bovine serum albumin (BSA) in phosphate-buffered saline (PBS) pH 7.3, samples were incubated with primary antibodies for 1 h in 1% BSA solution. Antibodies against the PsaD subunit of PS I and the CF_1 β subunit of ATP synthase were kindly provided by Jean-David Rochaix and Shimon Gepstein. Secondary antibody was an affinity-purified polyclonal goat anti-rabbit IgG conjugated with 20 nm gold (BBInternational, Cardiff, UK). All reactions were performed in the dark at room temperature.

Images acquired in the contact mode were obtained using PicoSPM (Molecular Imaging, Phoenix, AZ) equipped with a 7 μm scanner. Oxide-sharpened Si_3N_4-cantilevered tips (k = 0.06 N/m) were purchased from Digital Instruments (Digital Instruments, Santa Barbara, CA). Images were recorded with forces set minimally above lift-off values, at 1–5 Hz, and were acquired as 512 × 512 pixel arrays. Tapping mode SFM was carried out with Nanoscope IIIa (Digital Instruments) equipped with a 12 μm scanner, using etched silicon cantilevers (k = 42 N/m; Olympus, Tokyo, Japan). Drive amplitudes were 100–150 mV and force set points were 1–2 V. Scans were acquired at 1.1 Hz as 512 × 512 pixel arrays.

The least square numerical fitting of the particle size and height histograms to a sum of two-variable Gaussians

$$P = A_h \cdot \frac{e^{-2(h-h_p)/w_{1/2}^2}}{w_{1/2}\sqrt{\pi/2}} \cdot A_d \cdot \frac{e^{-2(d-d_p)/w_{1/2}^2}}{w_{1/2}\sqrt{\pi/2}}$$

yielded mean particle height, h_p, diameter, d_p and density of the generated particle classes.

Scanning EM

Samples were fixed with 2% (v/v) glutaraldehyde in 0.1 M Na cacodylate buffer pH 7.4, post-fixed in 1% (w/v) osmium tetraoxide, dehydrated in a graded ethanol series and critical point dried. Samples were coated with a gold-Pt film by sputtering and viewed with a JEOL 6400 scanning electron microscope.

Chlorophyll fluorescence

Maximal photochemical yield of PS II, Φ_p^{max}, was determined under conditions used for SFM from measurements of chlorophyll fluorescence using an FL-100 double-modulation fluorometer (Photon Systems Instruments, Brno, Czechia), as described earlier (Nedbal *et al*., 1999). PS II antenna heterogeneity (Melis and Homan, 1976) was assessed by measurements of chlorophyll fluorescence induction in buffer solution containing 10 μM DCMU. Least square numerical fitting of the measured kinetics to a model fluorescence transient (Joliot and Joliot, 1964; Lavergne and Trissl, 1995) was performed as in Nedbal *et al*. (1999) and yielded the functional cross-sections of PS II ($\sigma_{PSII}\alpha$ and $\sigma_{PSII}\beta$), and the relative abundance of PS IIα and PS IIβ. All measurements were conducted at 20°C.

Acknowledgements

We thank Dr Eugenia Klein for her help with the scanning EM studies, Dr Uri Pick for his assistance in the isolation of the chloroplasts, Drs Shimon Gepstein and Jean-David Rochaix for providing antibodies against ATP synthase and PS I, Mr Vladimir Kiss for his help with image analysis, and Drs Marvin Edelman, Shmuel Malkin, Abraham Minsky, Itzhak Ohad and Ellen Wachtel for helpful discussions. We are much obliged to the anonymous referees for their helpful comments and suggestions. This work was supported by the Avron-Wilstätter Minerva Centre for Research in Photosynthesis. Z.R. is an Allon fellow and incumbent of the Abraham and Jennie Fialkow Career Development Chair.

References

Albertsson,P.A. (2001) A quantitative model of the domain structure of the photosythetic membrane. *Trends Plant Sci.*, **6**, 349–354.

Albertsson,P.A. and Yu,S.G. (1988) Heterogeneity among photosystem IIα. Isolation of thylakoid membrane vesicles with different functional antennae size of photosystem IIα. *Biochim. Biophys. Acta*, **936**, 215–221.

Allen,J.F. (1992) Protein phosphorylation in regulation of photosynthesis. *Biochim. Biophys. Acta*, **1098**, 275–335.

Allen,J.F. and Forsberg,J. (2001) Molecular recognition in thylakoid structure and function. *Trends Plant Sci.*, **6**, 317–326.

Anderson,J.M. (1999) Insights into the consequences of grana stacking of thylakoid membranes in vascular plants: a personal perspective. *Austr. J. Plant Physiol.*, **26**, 625–639.

Arvidsson,P.O. and Sundby,C. (1999) A model for the topology of the chloroplast thylakoid membrane. *Austr. J. Plant Physiol.*, **26**, 687–694.

Avron,M. (1960) Photophosphorylation by Swiss-chard chloroplasts. *Biochim. Biophys. Acta*, **40**, 257–272.

Barber,J. (1980) An explanation for the relationship between salt-induced thylakoid stacking and the chlorophyll fluorescence changes associated with changes in spillover energy from photosystem II to photosystem I. *FEBS Lett.*, **118**, 1–10.

Binnig,G., Quate,C.F. and Gerber,C. (1986) Atomic force microscope. *Phys. Rev. Lett.*, **56**, 930–933.

Boekema,E.J., Jensen,P.E., Schlodder,E., van Breemen,J.F.L., van Roon, H., Scheller,H.V. and Dekker,J.P. (2001) Green plant photosystem I binds light-harvesting complex I on one side of the complex. *Biochemistry*, **40**, 1029–1036.

Boichenko,V.A. (1998) Action spectra and functional antenna sizes of photosystems I and II in relation to the thylakoid membrane organization and pigment composition. *Photosynth. Res.*, **58**, 163–174.

Boichenko,V.A., Bader,K.P., Klimov,V.V. and Schmidt,G.H. (1997) Mass spectrometric study of photosystem II heterogeneity in oxygen and nitrogen production: effects of magnesium and of phosphorylation of pea thylakoids. *Photosynth. Res.*, **52**, 49–55.

Chow,W.S. (1999) Grana formation: entropy-assisted local order in chloroplasts? *Austr. J. Plant Physiol..*, **26**, 641–647.

Drepper,F., Carlberg,I., Andersson,B. and Haehnel,W. (1993) Lateral

diffusion of integral membrane protein: Monte Carlo analysis of the migration of phosphorylated light-harvesting complex II in the thylakoid membrane. *Biochemistry*, **32**, 11915–11922.

Dunahay,T. and Staehelin,A.L. (1985) Isolation of photosystem I complexes from octylglucoside/SDS solubilized spinach thylakoids. *Plant Physiol.*, **78**, 606–613.

Fotiadis,D., Muller,D.J., Tsiotis,G., Hasler,L., Tittmann,P., Mini,T., Jeno,P., Gross,H. and Engel,A. (1998) Surface analysis of the photosystem I complex by electron and atomic force microscopy. *J. Mol. Biol.*, **283**, 83–94.

Genty,B., Briantias,J.M. and Baker,N.R. (1989) The relationship between the quantum yield of photosynthetic electron transport and quenching of chlorophyll fluorescence. *Biochim. Biophys. Acta*, **990**, 87–92.

Joliot,A. and Joliot,P. (1964) Etude cinétique de la réaction photochimique libérant l'oxygene au cours de la photosynthése. *C.R. Acad. Sci. Paris*, **258D**, 4622–4625.

Jordan,P., Fromme,P., Witt,H.T., Klukas,O., Saenger,W. and Krauss,N. (2001) Three-dimensional structure of cyanobacterial photosystem I at 2.5 Å resolution. *Nature*, **411**, 909–917.

Kitmitto,A., Holzenburg,A. and Ford,R.C. (1997) 2-Dimensional crystals of photosystem-I in higher-plant grana margins. *J. Biol. Chem.*, **272**, 19497–19501.

Kitmitto,A., Mustafa,A.O., Holzenburg,A. and Ford,R.C. (1998) Three-dimensional structure of higher plant photosystem I determined by electron crystallography. *J. Biol. Chem.*, **273**, 29592–29599.

Kuhlbrandt,W., Wang,D.A. and Fujiyoshi,Y. (1994) Atomic model of plant light-harvesting complex by electron crystallography. *Nature*, **367**, 614–621.

Lavergne,J. and Trissl,H.W. (1995) Theory of fluorescence induction in photosystem-II—derivation of analytical expressions in a model including exciton–radical-pair equilibrium and restricted energy-transfer between photosynthetic units. *Biophys. J.*, **68**, 2474–2492.

Mehta,M., Sarafis,V. and Critchley,C. (1999) Thylakoid membrane architecture. *Austr. J. Plant Physiol.*, **26**, 709–716.

Melis,A. and Homan,P.H. (1976) Heterogeneity of the photochemical centers in system II of chloroplasts. *Photochem. Photobiol.*, **23**, 343–350.

Mullineaux,C.W., Tobin,M.J. and Jones,G.R. (1997) Mobility of photosynthetic complexes in thylakoid membranes. *Nature*, **390**, 421–424.

Mustardy,L. (1996) Development of thylakoid membrane stacking. In Ort,D.R. and Yocum,C.F. (eds), *Oxygenic Photosynthesis: The Light Reactions*, Vol. 4. Kluwer Academic Publishers, Dodrecht, The Netherlands, pp. 59–68.

Mustardy,L. and Brangeon,J. (1978) 3-Dimensional chloroplast infrastructure: developmental aspects. In Akoyonoglou,G. (ed.), *Chloroplast Development*. Elsevier North-Holland Biomedical Press, Amsterdam, The Netherlands, pp. 489–494.

Nedbal,L., Trtilek,M. and Kaftan,D. (1999) Flash fluorescence induction: a novel method to study regulation of photosystem II. *J. Photochem. Photobiol.*, **48**, 154–157.

Olive,J. and Vallon,O. (1991) Structural organization of the thylakoid membrane—freeze-fracture and immunocytochemical analysis. *J. Electron Microsc. Tech.*, **18**, 360–374.

Reich,Z., Kapon,R., Nevo,R., Pilpel,Y., Zmora,S. and Scolnik,Y. (2001) Scanning force microscopy in the applied biological sciences. *Biotech. Adv.*, **19**, 451–485.

Samson,G. and Bruce,D. (1995) Complementary changes in absorption cross-sections of photosystems-I and photosystems-II due to phosphorylation and Mg^{2+}-depletion in spinach thylakoids. *Biochim. Biophys. Acta*, **1232**, 21–26.

Scheller,H.V., Jensen,P.E., Haldrup,A., Lunde,C. and Knoetzel,J. (2001) Role of subunits in eukaryotic photosystem I. *Biochim. Biophys. Acta*, **1507**, 41–60.

Staehelin,L.A. (1976) Reversible particle movements associated with unstacking and restacking of chloroplast membranes *in vitro*. *J. Cell Biol.*, **71**, 135–158.

Staehelin,L.A. (1986) Chloroplast structure and supramolecular organization of photosynthetic membranes. In Staehelin,L.A. and Arntzen,C.J. (eds), *Photosynthesis III: Photosynthetic Membranes and Light-harvesting Systems*. Springer-Verlag, Berlin, Germany, pp. 1–84.

Staehelin,L.A. and van der Staay,G.W.M. (1996) Structure, composition, functional organization and dynamic properties of thylakoid membranes. In Ort,D.R. and Yocum,C.F. (eds), *Oxygenic Photosynthesis: The Light Reactions*, Vol. 4. Kluwer Academic Publishers, Dodrecht, The Netherlands, pp. 11–30.

Stys,D. (1995) Stacking and separation of photosystem I and photosystem II in plant thylakoid membranes: a physico-chemical view. *Physiol. Plant.*, **95**, 651–657.

Trissl,H.-W. and Wilhelm,C. (1993) Why do thylakoid membranes form grana stacks? *Trends Biochem. Sci.*, **18**, 415–419.

Zhouni,A., Witt,H.-T., Kern,J., Fromme,P., Krauss,N., Saenger,W. and Orth,P. (2001) Crystal structure of photosystem II from *Synechococcus elongatus* at 3.8 Å resolution. *Nature*, **409**, 739–743.

Received June 4, 2002; revised September 17, 2002; accepted September 30, 2002